12-29-2020

A Generalized Bayesian Approach for Localizing Static Natural Obstacles on Unpaved Roads

Yoshito Kinoshita
Komatsu, yoshito_kinoshita@global.komatsu

Josiah Steckenrider
United States Military Academy, john.steckenrider@westpoint.edu

Ioannis Papakis
Virginia Polytechnic Institute and State University, iopapakis@vt.edu

Tomonari Furukawa
University of Virginia, tf4rp@virginia.edu

Recommended Citation

Y. Kinoshita, J. Steckenrider, I. Papakis and T. Furukawa, "A Generalized Bayesian Approach for Localizing Static Natural Obstacles on Unpaved Roads," 2020 IEEE International Symposium on Safety, Security, and Rescue Robotics (SSRR), Abu Dhabi, UAE, 2020, pp. 283-289. doi: https://doi.org/10.1109/SSRR50563.2020.9292600

2020 IEEE International Symposium on
Safety, Security, and Rescue Robotics (SSRR)
November 4-6, Abu Dhabi, UAE

A Generalized Bayesian Approach for Localizing Static Natural Obstacles on Unpaved Roads

Yoshito Kinoshita[1], Josiah Steckenrider[2], Ioannis Papakis[3] and Tomonari Furukawa[4]

Abstract— **This paper presents an approach that implements sensor fusion and recursive Bayesian estimation (RBE) to improve a vehicle's ability to perform obstacle detection and localization in unpaved road environments. The proposed approach utilizes RADAR, LiDAR and stereovision fully for sensor fusion to detect and localize static natural obstacles. Each sensor is characterized by a probabilistic sensor model which quantifies level of confidence (LOC) and probability of detection (POD) associatively. Deploying these sensor models enables the fusion of heterogeneous sensors without extensive formulations and with the incorporation of each sensor's strengths. An Extended Kalman filter (EKF) is formulated and implemented for robust and computationally efficient RBE of obstacles' locations while a sensor-equipped vehicle moves and observes them. Results with a test vehicle show the successful detection and localization of a static natural object on an unpaved road has demonstrated the effectiveness of the proposed approach.**

I. Introduction

The last couple of decades have seen the development of new perception technologies following the growing demand for Advanced Driver-Assistant Systems (ADAS) and autonomous vehicle operation. Among the most intensively studied topics is the recognition of obstacles in the direction of travel. Obstacles of highest concern are typically pedestrians and other objects on paved roads [1], [2], which are often distinct or dynamic and thus relatively easy to recognize. Static natural obstacles on unpaved roads such as rocks, which are of interest in this paper, originate from the surrounding environment and can be highly unstructured and indistinguishable. It is therefore imperative that off-road vehicles have sufficiently advanced capabilities to detect and localize such obstacles.

To date, most past work associated with autonomous vehicles has focused on detecting obstacles on paved roads. Recent work [3], [4], [5] showed advances in detection and tracking of pedestrians and vehicles in front of a vehicle using multiple sensors such as RADAR, LiDAR, and cameras. Chadwick, et al. [6] developed a system with a RADAR sensor and two cameras of different focal lengths for distant vehicle detection. Other studies [7], [8], [9] focused on the detection of small obstacles on paved roads using stereovision and machine learning techniques. In addition, Xue, et al. [10] developed a technique to detect small obstacles via multi-layer image edge detection using a monocular camera.

Meanwhile, obstacle detection on unpaved roads has been studied primarily in mining and military domains. Automatic human detection techniques for mining environments using millimeter-wave RADAR sensors have existed now for a few decades [11]. Manduchi, et al. [12] classified terrains and detected obstacles in short range using LiDAR and camera sensors. However, little research covers the detection and localization of distant natural obstacles on unpaved roads. This is largely due to the ill-posed nature of such detection and localization problems.

This paper presents a generalized approach for improving vehicle-based obstacle detection and localization in unpaved road environments. The key contributions of the proposed approach are: 1) the probabilistic modeling, fusion and deployment of RADAR, LiDAR and stereo-camera sensors for detection of static natural obstacles on unpaved roads, and 2) the formulation of an extended Kalman filter (EKF) based framework for obstacle localization using this fused sensory input. These unique contributions aim to overcome the significant irregularities associated with off-road obstacle localization. Each sensor is characterized by a probabilistic sensor model proposed by Furukawa, et al [13], which quantifies level of confidence (LOC) and probability of detection (POD) associatively. By deploying such sensor models, the proposed approach enables heterogeneous sensor fusion without the need for extensive formulations and with the incorporation of each sensor's strengths. The proposed EKF-based formulation is extracted from generalized recursive Bayesian estimation (RBE) such that the location of obstacles during vehicle operation can be robustly estimated even though such obstacle localization is challenging under traditional approaches.

This paper is organized as follows. The next section deals with the general framework of RBE that incorporates limited sensor capability. The proposed modeling and fusion of the three sensors and EKF-based localization are presented in Section III. Experimental validation with a test vehicle is presented in Section IV. Conclusions and future work are summarized in the final section.

II. Recursive Bayesian Estimation

A. Object and Vehicle Models

Consider a static obstacle (henceforth referred to by the more general term "object") of interest o with its unknown

[1]Yoshito Kinoshita is with Komatsu, Ltd., Japan. yoshito_kinoshita@global.komatsu
[2]Josiah Steckenrider is with Department of Civil and Mechanical Engineering, United States Military Academy, NY, USA. john.steckenrider@westpoint.edu
[3]Ioannis Papakis is with Department of Mechanical Engineering, Virginia Tech, Blacksburg, VA, USA. ioannis1@vt.edu
[4]Tomonaari Furukawa is with Department of Mechanical and Aerospace Engineering, University of Virginia, VA, USA. tomonari@virginia.edu

978-0-7381-1123-0/20/$31.00 ©2020 IEEE

global state given by $\mathbf{x}^o \in \mathcal{X}^o$. This object is observed by a robot vehicle r, the global state of which evolves with the motion model

$$\mathbf{x}_k^r = \mathbf{f}^r\left(\mathbf{x}_{k-1}^r, \mathbf{u}_k^r, \mathbf{w}_k^r\right), \tag{1}$$

where $\mathbf{x}_k^r \in \mathcal{X}^r$ and $\mathbf{u}_k^r \in \mathcal{U}^r$ represent the state and control input of the vehicle at time step k, respectively, and $\mathbf{w}_k^r \in \mathcal{W}^r$ is vehicle system noise. The ith sensor which localizes the vehicle is generically described by

$${}^{s_i}\mathbf{z}_k^r = {}^{s_i}\mathbf{h}^r\left(\mathbf{x}_k^r, {}^{s_i}\mathbf{v}_k^r\right), \tag{2}$$

where ${}^{s_i}\mathbf{z}_k^r$ and ${}^{s_i}\mathbf{v}_k^r$ are the observed vehicle pose and the observation noise respectively.

To detect and localize an object, the vehicle uses sensors which each have an "observable region" determined by the sensor's physical capability. For example, the observable region of an optical sensor would be its field of view (FOV). Let the probability of detecting an object with state $\mathbf{x}^o$ given the robot vehicle's state $\mathbf{x}_k^r$ and the parameters associated with the jth sensor $\boldsymbol{\pi}^{s_j}$ be denoted $P_d\left(\mathbf{x}^o|\mathbf{x}_k^r; \boldsymbol{\pi}^{s_j}\right)$. The observable region of the sensor for the object ($j \in \mathcal{I}^o$) can then be expressed as

$${}^{s_j}\mathcal{X}^o = \left\{\mathbf{x}^o | 0 < P_d\left(\mathbf{x}^o|\mathbf{x}_k^r; \boldsymbol{\pi}^{s_j}\right) \leq 1\right\}.$$

Accordingly, the model of the jth sensor is given by

$${}^{s_j}\mathbf{z}_k^o = \begin{cases} {}^{s_j}\mathbf{h}^o\left(\mathbf{x}^o, \mathbf{x}_k^r, {}^{s_j}\mathbf{v}_k^o\right) & \mathbf{x}^o \in^{s_j} \mathcal{X}^o \\ \emptyset & \text{otherwise} \end{cases} \tag{3}$$

where ${}^{s_j}\mathbf{v}_k^o$ represents observation noise, and $\emptyset$ denotes the empty set.

B. Recursive Bayesian Estimation and Sensor Fusion

RBE is used to estimate belief about an object or a vehicle itself in the global coordinate frame. Under RBE, belief is represented by probability density function (PDF)s and recursively updated through prediction and correction. Consider a generic scenario where a sequence of self-observations by the jth sensor on the vehicle from time step 1 to k is denoted as ${}^{s_i}\tilde{\mathbf{z}}_{1:k}^r \equiv \left\{{}^{s_i}\tilde{\mathbf{z}}_\kappa^r | \forall \kappa \in \{1, ..., k\}\right\}$, whereas observations on the object by the jth sensor are given by ${}^{s_j}\tilde{\mathbf{z}}_{1:k}^o \equiv \left\{{}^{s_j}\tilde{\mathbf{z}}_\kappa^r | \forall \kappa \in \{1, ..., k\}\right\}$. Note here that $\tilde{(\cdot)}$ represents an instance of a corresponding variable $(\cdot)$. Given the initial belief $p\left(\mathbf{x}_0^r, \mathbf{x}^o\right)$, a sequence of observations by sensors for self-localization ${}^{s}\tilde{\mathbf{z}}_{1:k}^r \equiv \left\{{}^{s_i}\tilde{\mathbf{z}}_{1:k}^r | \forall i \in \mathcal{I}^r\right\}$ and object localization ${}^{s}\tilde{\mathbf{z}}_{1:k}^o \equiv \left\{{}^{s_j}\tilde{\mathbf{z}}_{1:k}^o | \forall j \in \mathcal{I}^o\right\}$, and an input $\tilde{\mathbf{u}}_{1:k}^r$, the vehicle and the object belief at time step k, $p\left(\mathbf{x}_k^r, \mathbf{x}^o | {}^{s}\tilde{\mathbf{z}}_{1:k}^r, {}^{s}\tilde{\mathbf{z}}_{1:k}^o, \tilde{\mathbf{u}}_{1:k}^r\right)$, is given by a prediction followed by correction according to the following formulations.

Prediction: Computes the vehicle and object belief at k from the belief updated at $k-1$ by the Chapman-Kolmogorov equation:

$$\begin{aligned} &p\left(\mathbf{x}_k^r, \mathbf{x}^o | {}^{s}\tilde{\mathbf{z}}_{1:k-1}^r, {}^{s}\tilde{\mathbf{z}}_{1:k-1}^o, \tilde{\mathbf{u}}_{1:k}^r\right) \\ &= \int_{\mathcal{X}^r} p\left(\mathbf{x}_k^r | \mathbf{x}_{k-1}^r, \tilde{\mathbf{u}}_k^r\right) p\left(\mathbf{x}_{k-1}^r, \mathbf{x}^o | {}^{s}\tilde{\mathbf{z}}_{1:k-1}^r, {}^{s}\tilde{\mathbf{z}}_{1:k-1}^o, \tilde{\mathbf{u}}_{1:k-1}^r\right) d\mathbf{x}_k^r, \end{aligned} \tag{4}$$

where $p\left(\mathbf{x}_k^r | \mathbf{x}_{k-1}^r, \tilde{\mathbf{u}}_k^r\right)$ comes from a Markovian motion model defined by Eq. (1).

Correction: Computes the vehicle and object belief given the predicted belief and new observations ${}^{s}\tilde{\mathbf{z}}_k^r$ and ${}^{s}\tilde{\mathbf{z}}_k^o$:

$$\begin{aligned} &p\left(\mathbf{x}_k^r, \mathbf{x}^o | {}^{s}\tilde{\mathbf{z}}_{1:k}^r, {}^{s}\tilde{\mathbf{z}}_{1:k}^o, \tilde{\mathbf{u}}_{1:k}^r\right) \\ &= \frac{l(\mathbf{x}_k^r, \mathbf{x}^o | {}^{s}\tilde{\mathbf{z}}_k^r, {}^{s}\tilde{\mathbf{z}}_k^o) p\left(\mathbf{x}_k^r, \mathbf{x}^o | {}^{s}\tilde{\mathbf{z}}_{1:k-1}^r, {}^{s}\tilde{\mathbf{z}}_{1:k-1}^o, \tilde{\mathbf{u}}_{1:k}^r\right)}{\int_{\mathcal{X}^r} l\left(\mathbf{x}_k^r, \mathbf{x}^o | {}^{s}\tilde{\mathbf{z}}_k^r, {}^{s}\tilde{\mathbf{z}}_k^o\right) p\left(\mathbf{x}_k^r, \mathbf{x}^o | {}^{s}\tilde{\mathbf{z}}_{1:k-1}^r, {}^{s}\tilde{\mathbf{z}}_{1:k-1}^o, \tilde{\mathbf{u}}_{1:k}^r\right) d\mathbf{x}_{k-1}^r}, \end{aligned} \tag{5}$$

where $l\left(\mathbf{x}_k^r, \mathbf{x}^o | {}^{s}\tilde{\mathbf{z}}_k^r, {}^{s}\tilde{\mathbf{z}}_k^o\right)$ represents the likelihood of $\mathbf{x}_k^r$ and $\mathbf{x}^o$ given observations ${}^{s}\tilde{\mathbf{z}}_k^r$ and ${}^{s}\tilde{\mathbf{z}}_k^o$, which can be broken down into the object and vehicle observation likelihoods:

$$\begin{aligned} &l\left(\mathbf{x}_k^r, \mathbf{x}^o | {}^{s}\tilde{\mathbf{z}}_k^r, {}^{s}\tilde{\mathbf{z}}_k^r\right) \\ &\qquad = \prod_j \prod_i l\left(\mathbf{x}^o | {}^{s_j}\tilde{\mathbf{z}}_k^o, \mathbf{x}_k^r\right) l\left(\mathbf{x}_k^r | {}^{s_i}\tilde{\mathbf{z}}_k^r, {}^{s_j}\tilde{\mathbf{z}}_k^o\right). \end{aligned} \tag{6}$$

The formulation of the object observation likelihood differs depending on whether or not the object is detected. Let the detectable region of the jth sensor for object observation, defined as the region within which the sensor finds the object with some confidence, be given by

$${}^{s_j}\mathcal{X}_d^o = \left\{\mathbf{x}^o | {}^{s_j}\epsilon^o < P_d\left(\mathbf{x}^o | \mathbf{x}_k^r, \boldsymbol{\pi}^{s_j}\right) \leq 1\right\} \subset {}^{s_j}\mathcal{X}^o,$$

where ${}^{s_j}\epsilon^o$ is a positive confidence threshold which determines the detection of the object. Given an observation ${}^{s_j}\tilde{\mathbf{z}}_k^o$, the object observation likelihood is then

$$l\left(\mathbf{x}^o | {}^{s_j}\tilde{\mathbf{z}}_k^o, \tilde{\mathbf{x}}_k^r\right) = \begin{cases} p\left(\mathbf{x}^o | {}^{s_j}\tilde{\mathbf{z}}_k^o, \mathbf{x}_k^r; \boldsymbol{\pi}^{s_j}\right) & {}^{s_j}\tilde{\mathbf{z}}_k^o \in {}^{s_j}\mathcal{X}_d^o \\ 1 - P_d\left(\mathbf{x}^o | \mathbf{x}_k^r; \boldsymbol{\pi}^{s_j}\right) & \text{otherwise} \end{cases}, \tag{7}$$

where the upper and lower formulas provide likelihoods with detection and non-detection events, respectively [13]. If the observed object is within the detectable region, the likelihood is generally uni-modal and often near-Gaussian PDF around the observed object state. Otherwise, the likelihood becomes heavily non-Gaussian.

While these formulations are comprehensive, their direct implementation using non-Gaussian techniques such as the grid-based method significantly suffers from computational cost. However, it is essential that computation be fast since detection and localization take place during vehicle operation. This motivates the use of the EKF as an online Gaussian recursive Bayesian estimator.

III. Proposed Obstacle Detection and Localization Approach

A. Overview

Figure 1 shows an overview of the proposed obstacle detection and localization approach. The framework takes the form of an EKF for computationally efficient localization and deploys LiDAR, RADAR and stereo camera sensing for

2020 IEEE International Symposium on
Safety, Security, and Rescue Robotics (SSRR)
November 4-6, Abu Dhabi, UAE

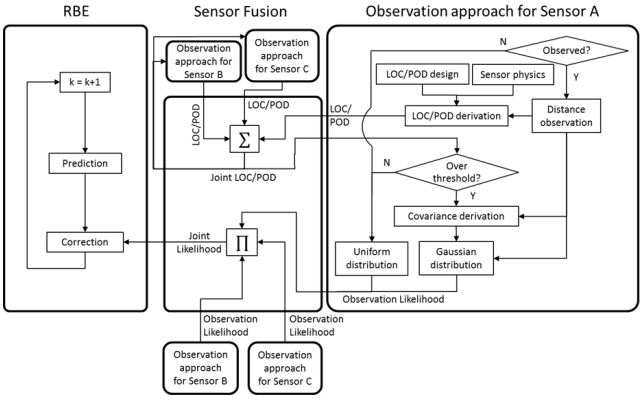

Fig. 1. Proposed obstacle detection and localization approach

robust detection of static natural obstacles. Each sensor is represented by the abstract placeholder "Sensor A" which generalizes sensor formulation and processing. Once an object has been detected by a sensor, the LOC is calculated according to a predetermined sensor-intrinsic LOC curve. The POD is calculated by adding the LOCs of all the sensors. After calculating the observation likelihood of each sensor using the POD, the joint likelihood of all the sensors can be obtained by fusing the observation likelihoods. If the sensor does not detect an object or if the POD value is lower than some threshold, the uniform distribution is returned as an observation likelihood.

B. Proposed Generalized Sensor Modeling

The proposed generalized sensor model is mathematically presented as follows. In order to use the EKF, the observation likelihood of the jth sensor, Eq. (7), is constrained to be Gaussian:

$$l\left(\mathbf{x}^o \middle| {}^{s_j}\tilde{\mathbf{z}}_k^o, \mathbf{x}_k^r\right) = \begin{cases} \mathcal{N}\left({}^{s_j}\tilde{\mathbf{z}}_k^o, {}^{s_j}\mathbf{\Sigma}_k^{ov}\right) & {}^{s_j}\tilde{\mathbf{z}}_k^o \in {}^{s_j}\mathcal{X}_d^o \\ \mathcal{U}\left(\mathcal{X}^o\right) & \text{otherwise} \end{cases} . \quad (8)$$

Here, the non-detection likelihood $\mathcal{U}\left(\mathcal{X}^o\right)$ is a uniform distribution over the object space $\mathcal{X}^o$. If the observed object is within the detectable region, the likelihood can be approximated as a uni-modal Gaussian PDF whose mean is given by the observation ${}^{s_j}\tilde{\mathbf{z}}_k^o$. If not, the likelihood provides no new information on the object.

The covariance of the observation likelihood is given by

$${}^{s_j}\mathbf{\Sigma}_k^{ov} = \frac{w_j}{L_c^{s_j}} {}^{\{G\}}_{\{R\}}\mathbf{T} \cdot {}^{\{R\}}\mathbf{U}\left({}^{s_j}\tilde{\mathbf{z}}_k^o\right) \cdot {}^{\{G\}}_{\{R\}}\mathbf{T}^\top, \quad (9)$$

where w_j is a scaling factor of the jth sensor, ${}^{\{G\}}_{\{R\}}\mathbf{T}$ is a transformation matrix from the global frame $\{G\}$ to the robot frame $\{R\}$, ${}^{\{R\}}\mathbf{U}\left({}^{s_j}\tilde{\mathbf{z}}_k^o\right)$ is a unitary matrix, the elements of which are determined by the uncertainty in range and bearing of the jth sensor's object observation, and $L_c^{s_j}$ is the LOC of the jth sensor. The LOC is a quantity of each sensor and is defined as

$$L_c^{s_j} = L_{c0}^{s_j} - f\left(\left\|{}^{s_j}\tilde{\mathbf{z}}_k^o\right\|; a_j\right). \quad (10)$$

$L_c^{s_j} = {}^{s_j}\epsilon^o$ when ${}^{s_j}\tilde{\mathbf{z}}_k^o$ is at the border of ${}^{s_j}\mathcal{X}_d^o$. In the equation, $\boldsymbol{\pi}^{s_j} \equiv \left[L_{c0}^{s_j}, a_j\right]$ is the aforementioned sensor parameter vector and f is formulated such that the LOC decreases as the distance to the object increases. The POD of the jth sensor, $P_d^{s_j}$, is related to the LOC by

$$P_d^{s_j} = \min\left\{L_c^{s_j}, 1\right\}. \quad (11)$$

Figure 2 illustrates the observation likelihood constructed for each of the sensors addressed in this paper. While the three-dimensional (3D) LiDAR and RADAR both reliably measure range, the stereo camera can achieve high resolution in bearing measurement. RADAR detects objects at the longest ranges, but 3D LiDAR measures range more accurately. The advantage of generalized sensor modeling is that three very different sensors can be modeled using a relatively low number of parameters.

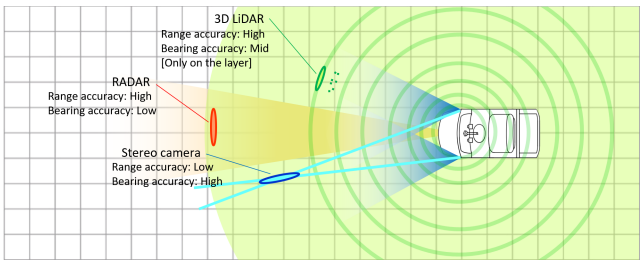

Fig. 2. Observation likelihood for each sensor

C. Sensor Fusion and EKF Estimation

Because the observation likelihoods can be represented by Gaussian distributions, the proposed approach can use an EKF approach for RBE. Under the EKF, the mean and covariance of the vehicle state are propagated in prediction by

$$\hat{\mathbf{x}}_{k|k-1}^r = \mathbf{f}^r\left(\hat{\mathbf{x}}_{k-1|k-1}^r, \tilde{\mathbf{u}}_k^r\right), \quad (12a)$$

$$\mathbf{\Sigma}_{k|k-1}^r = \nabla_r \mathbf{f}^r \mathbf{\Sigma}_{k-1|k-1}^r \nabla_r \mathbf{f}^{r\top} + \mathbf{\Sigma}_{k-1}^{rw}, \quad (12b)$$

where $\nabla_r \mathbf{f}^r$ is the Jacobian of the motion model $\mathbf{f}^r(\cdot)$ with respect to the vehicle evaluated at the estimate $\hat{\mathbf{x}}_{k-1|k-1}^r$. Correction is then given by:

$$\hat{\mathbf{x}}_{k|k}^r = \hat{\mathbf{x}}_{k|k-1}^r + \sum_i {}^{s_i}\mathbf{W}_k^r \left[{}^{s_i}\tilde{\mathbf{z}}_k^r - {}^{s_i}\mathbf{h}^r\left(\hat{\mathbf{x}}_{k|k-1}^r\right)\right], \quad (13a)$$

$$\mathbf{\Sigma}_{k|k}^r = \mathbf{\Sigma}_{k|k-1}^r - \mathbf{\Sigma}_k^i, \quad (13b)$$

where

$$\mathbf{\Sigma}_k^i = \sum_i {}^{s_i}\mathbf{W}_k^r \nabla_r {}^{s_i}\mathbf{h}^r \mathbf{\Sigma}_{k|k-1}^r \quad (14)$$

is the covariance of the joint observation likelihood of the sensors localizing the vehicle, and ${}^{s_i}\mathbf{W}_k^r$ is the Kalman gain given by

$${}^{s_i}\mathbf{W}_k^r = \nabla_r {}^{s_i}\mathbf{h}^{r\top}\left(\nabla_r {}^{s_i}\mathbf{h}^r \mathbf{\Sigma}_{k|k-1}^r \nabla_r {}^{s_i}\mathbf{h}^{r\top} + {}^{s_i}\mathbf{\Sigma}_k^{rv}\right)^{-1}. \quad (15)$$

Here, $\nabla_r {}^{s_i}\mathbf{h}^r$ is the Jacobian of ${}^{s_i}\mathbf{h}^r(\cdot)$ with respect to the vehicle at $\hat{\mathbf{x}}_{k|k-1}^r$. The proposed approach effectively uses

the estimated $\hat{\mathbf{x}}^r_{k|k}$ and $\mathbf{\Sigma}^r_{k|k}$ to represent vehicle belief for subsequent object localization.

With respect to object belief, the prediction stage is eliminated since the object is static. Instead, only correction (5) is used to update object belief using the EKF:

$$\hat{\mathbf{x}}^o_{k|k} = \hat{\mathbf{x}}^o_{k-1|k-1} + \sum_j {}^{s_j}\mathbf{W}^o_k \left[{}^{s_j}\tilde{\mathbf{z}}^o_k - {}^{s_j}\mathbf{h}^o\left(\hat{\mathbf{x}}^o_{k-1|k-1}, \hat{\mathbf{x}}^r_{k|k}\right)\right], \quad (16a)$$

$$\mathbf{\Sigma}^{o'}_{k|k} = \mathbf{\Sigma}^o_{k-1|k-1} - \mathbf{\Sigma}^j_k, \quad (16b)$$

where the covariance of the joint observation likelihood of the sensors localizing the object is

$$\mathbf{\Sigma}^j_k = \sum_j {}^{s_j}\mathbf{W}^o_k \nabla_o {}^{s_j}\mathbf{h}^o \mathbf{\Sigma}^o_{k-1|k-1}, \quad (17)$$

and the Kalman gain ${}^{s_j}\mathbf{W}^o_k$ is given by

$${}^{s_j}\mathbf{W}^o_k = \mathbf{\Sigma}^o_{k-1|k-1} \nabla_o {}^{s_j}\mathbf{h}^{o\top} \left(\nabla_o {}^{s_j}\mathbf{h}^o \mathbf{\Sigma}^o_{k-1|k-1} \nabla_o {}^{s_j}\mathbf{h}^{o\top} + {}^{s_j}\mathbf{\Sigma}^{ov}_k\right)^{-1} \quad (18)$$

Again, $\nabla_o {}^{s_j}\mathbf{h}^o$ is the Jacobian of ${}^{s_j}\mathbf{h}^o(\cdot)$ with respect to the object at $\hat{\mathbf{x}}^o_{k|k-1}$. Finally, the covariance of the object is updated by incorporating the uncertainty of the vehicle:

$$\mathbf{\Sigma}^o_{k|k} = \mathbf{\Sigma}^{o'}_{k|k} + \mathbf{\Sigma}^r_{k|k}. \quad (19)$$

The Gaussian PDF $\mathcal{N}\left(\hat{\mathbf{x}}^o_{k|k}, \mathbf{\Sigma}^o_{k|k}\right)$ defined by the mean and covariance coming from the EKF represents updated object belief in the global coordinate frame.

IV. Experimental Validation

Since its strength is in applicability to complex scenarios, it is essential to test and validate the proposed approach in a practical context. The proposed approach was applied to the detection of rocks at a quarry in Blacksburg, Virginia, USA. Figure 3 shows the vehicle and rocks used for evaluation. The test vehicle, a Ford Escape, was equipped with a 3D LiDAR sensor, a RADAR sensor and a stereo camera. The two rocks used for testing were native to the quarry environment. One had a color which varied significantly from its environment, whereas the other's brown color was similar to the environment. Both had a height of approximately 25 cm. The brown rock on the right, which is more difficult to detect, was used for the actual validation and was initially located approximately 60 m from the test vehicle. The vehicle was driven towards the rock at a constant speed.

(a) Test vehicle (b) Obstacles

Fig. 3. Experimental infrastructure

Table I lists major parameters used in the validations; Figure 4 shows the LOCs as a function of the distance from the vehicle to the rock obstacle. Note that, in Table I, $d = \|{}^s\tilde{\mathbf{z}}^o_k\|$. The covariances used to create the observation likelihoods of each sensor was specified by capturing their physical characteristics before testing. Standard edge detection, color detection, and clustering algorithms were used for detection by the LiDAR, stereo camera and RADAR sensors, respectively. It is also important to note here that the 3D LiDAR has limited capability in obstacle detection as illustrated in Figure 5. Due to the low resolution in horizontal scanning, non-detection events occur when the obstacle is located between scans.

TABLE I
Important Parameters of the Proposed Approach

Parameter	Value
FOV of RADAR [deg]	20 (Long-range), 60 (Mid-range)
FOV of LiDAR [deg]	360
FOV of Stereovision	50
Observation covariance (RADAR) [m, m; m, m]	[0.1d, 0.0; 0, 0.004d]
Observation covariance (LiDAR) [m, m; m, m]	[0.1d, 0.0; 0, 0.0003d]
Observation covariance (Stereovision) [m, m; m, m]	[1.0d, 0.0; 0, 0.0001d]
Detection by LiDAR	Edge detection
Detection by Stereovision	Color detection
Detection by RADAR	Clustering

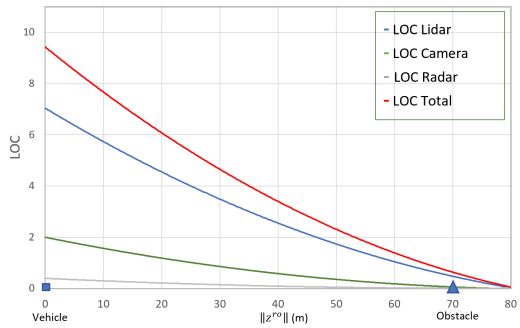

Fig. 4. LOC for each sensor and total

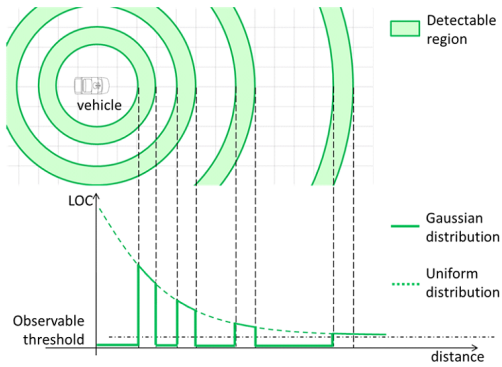

Fig. 5. Occurrence of no detection in 3D LiDAR

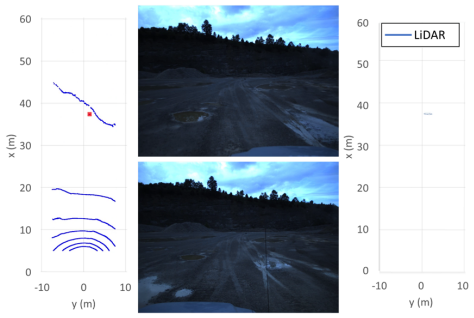

(a) Distance traveled = 22 m (Obstacle detected by 3D LiDAR only)

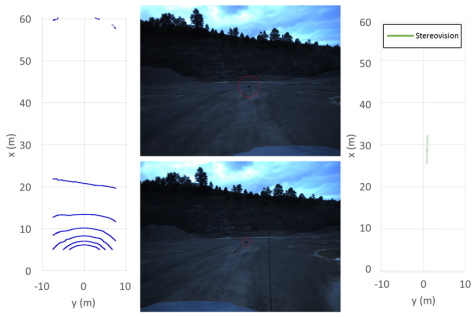

(b) Distance traveled = 30 m (Obstacle detected by stereo camera only)

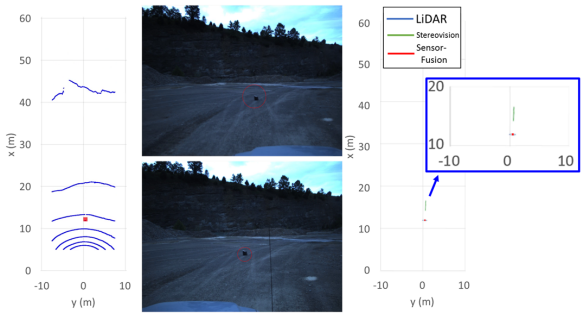

(c) Distance traveled = 58 m (Obstacle detected by LiDAR, stereo camera and RADAR)

Fig. 6. LiDAR/camera/RADAR images and observation likelihoods

Figure 6 shows a set of LiDAR/camera/RADAR images, the observation likelihood of each sensor, and the joint observation likelihood at different traveled distances. The solid ellipse represents the covariance of the observation likelihood, which is scaled to understand the change in covariance visually. No plot of the observation likelihood means that the obstacle was not detected by the sensor. In Figure 6(a), the obstacle is detected only by the 3D LiDAR as stereo-vision detection is unreliable since the color of the background is similar to that of the rock. The covariance shows less uncertainty in depth. This is because the 3D LiDAR is accurate in depth while the resolution is low. Figure 6(b), on the other hand, shows detection by the stereo camera only. While the obstacle is even closer, the 3D LiDAR is unable to detect the obstacle since no lines are scanned in the range between 20 m and 60 m. The covariance is thus oriented to show certainty in bearing. All sensors have detected the obstacle when the vehicle is approximately 12 m away from the obstacle as shown in Figure 6(c). The joint observation likelihood is seen to be highly certain due to the fusion of observation likelihoods created by sensors with different strengths.

Figure 7 shows a quantitative result of the proposed framework for the previously described test. Figure 7(a) shows the transition of the LOC by the LiDAR and the camera as well as the total LOC. The LOCs are initially zero since the obstacle is outside the detectable regions of both the sensors. The LOCs then increase as the vehicle approaches the obstacle. However, it is also clear that the LOC often becomes zero. This happens when detection does not occur. The LiDAR sensor can detect the obstacle well but only when a beam scans it. The detection capability of the camera depends on the obstacle's appearance in the image among many other factors. This instability is unavoidable in detection, emphasizing the importance of RBE, which constructs and updates belief based on past information.

Figure 7(b) shows the Kullback-Leibler (KL) divergence of the observation likelihood of each LiDAR and camera. Both the KL divergences gradually increase as the vehicle approaches the obstacle. The certainty of the observation clearly gets higher in proportion to the LOC.

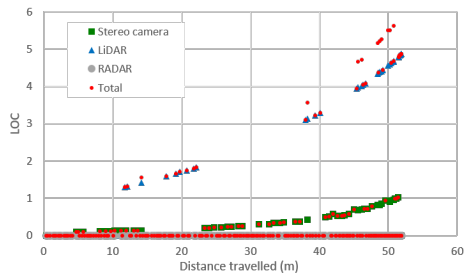

(a) LOCs vs. distance traveled

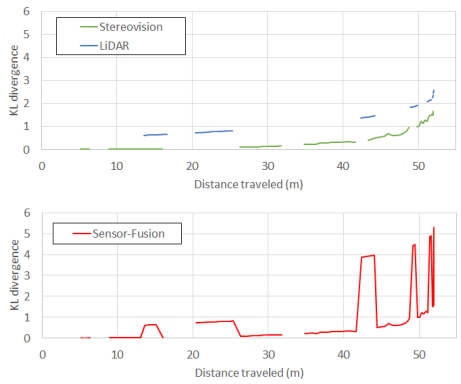

(b) KL divergence vs. distance traveled

Fig. 7. Quantitative result of obstacle observation

Figure 8 shows the result of the proposed localization approach where the blue and the red ellipses represent the scaled covariances of the vehicle and obstacle belief functions respectively. Figure 8(a) shows the initial belief

functions that have been constructed from prior knowledge whereas belief after the first detection are shown in Figure 8(b). It is clear that the corrected obstacle covariance is largely influenced by the LiDAR observation since the initial belief was so uncertain. This underscores the effectiveness of the proposed obstacle observation technique since it gives a guess on the obstacle location immediately after the first detection even though the LOC of the LiDAR sensor is still low. The camera detects the obstacle soon after, as shown in Figure 8(c), and thus estimation improves by means of sensor fusion. The proposed approach keeps reducing the uncertainty of both the vehicle and the obstacle as shown in Figure 8(d), until the vehicle reaches the obstacle.

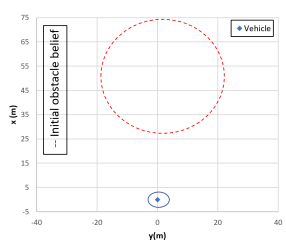

(a) Distance traveled = 0 m (Initial belief)

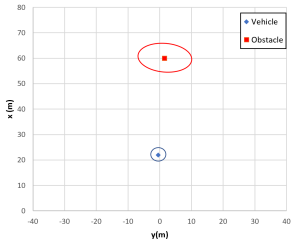

(b) Distance traveled = 22 m (Detected by LiDAR only)

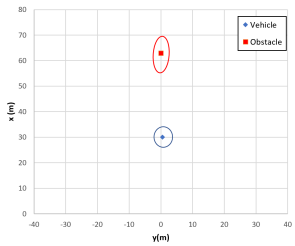

(c) Distance traveled = 30 m (Detected by stereo camera only)

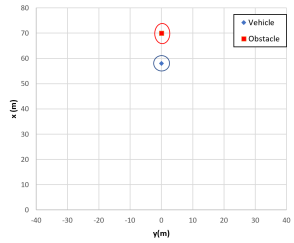

(d) Distance traveled = 58 m (Detected by LiDAR and stereo camera)

Fig. 8. Transition of observation likelihoods of vehicle and obstacle

Figure 9(a) shows the transition of the KL divergences of the vehicle and obstacle belief. The KL divergence of the vehicle belief fluctuates but is steady since only one Global Positioning System (GPS) sensor is used for self-localization. This GPS sensor has constant variance regardless of the measured vehicle position. The KL divergence of the obstacle belief keeps increasing regardless of whether or not it is detected by the sensors because belief is constantly updated by RBE. The effect of the sensor fusion is clearly seen, as the KL divergence of the obstacle belief increases dramatically after 12 and 38 meters have been traveled. This is because LiDAR detected the obstacle at 12 m for the first time, and both the LiDAR and stereo camera detected the obstacle for the first time. The estimation errors relative to ground truth are shown in Figure 9(b); from this it is evident that the vehicle is localized to within one meter, while obstacle localization error expectedly decreases to zero over the distance traveled.

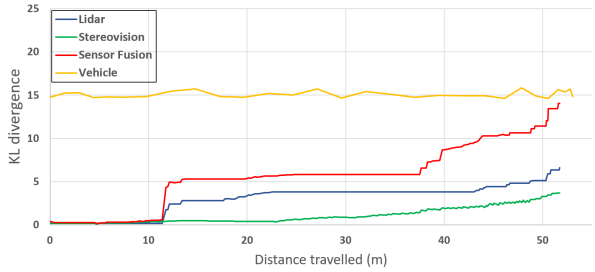

(a) KL divergence

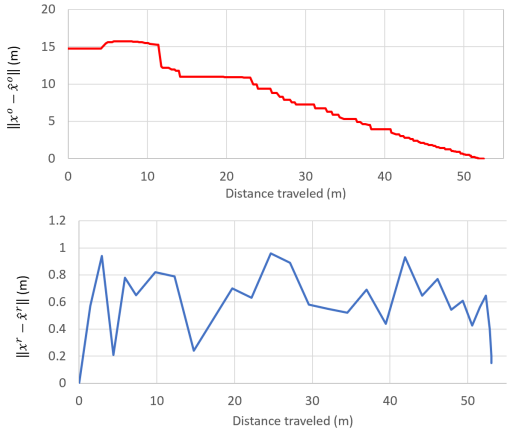

(b) Localization errors

Fig. 9. KL divergence and errors of vehicle and obstacle beliefs vs. distance travelled

V. Conclusions

This paper has presented an approach that implements a sensor-fusion-augmented EKF framework to improve vehicular obstacle detection and localization in unpaved road environments. The key contributions of the proposed approach include probabilistic modeling, fusion, and deployment of RADAR, LiDAR and stereo-camera sensors for detection of static natural obstacles and the formulation of an EKF based framework for their localization. Results with a test vehicle show the successful detection and localization of a static natural obstacle on an unpaved road. It is demonstrated that KL divergence formulated for obstacle belief continually increases as different sensor observations are consecutively added. Furthermore, as expected, certainty and accuracy of obstacle belief increases as the sensor-equipped vehicle approaches it. This framework proves to be successful in a highly unstructured domain where automation is difficult and existing approaches are generally insufficient.

The paper has focused on detecting and localizing a static natural obstacle on an unpaved road and much work is still left open. Ongoing topics that were not covered include the detection of multiple and/or dynamic natural obstacles, detailed obstacle detection algorithms, and vehicle localization using multiple sensors. These topics will be published in the future through conferences and journal special issues associated with such developing technologies.

REFERENCES

[1] Chen, Yaran; Zhao, Dongbin; Lv, Le; Zhang, Qichao. Multi-task learning for dangerous object detection in autonomous driving. Information Sciences. 2018 Volume: 432 559-571.

[2] Van Brummelen, Jessica; OBrien, Marie; Gruyer, Dominique; Najjaran, Homayoun. Autonomous vehicle perception: The technology of today and tomorrow. Transportation Research Part C. 2018 Volume: 89 384-406.

[3] Chen, Xiaozhi; Ma, Huimin; Wan, Ji; Li, Bo; Xia, Tian. Multi-view 3D Object Detection Network for Autonomous Driving. 2017 IEEE Conference on Computer Vision and Pattern Recognition (CVPR) 2017 6526-6534.

[4] Chavez-Garcia, Ricardo Omar; Aycard, Olivier. Multiple Sensor Fusion and Classification for Moving Object Detection and Tracking. IEEE Transactions on Intelligent Transportation Systems 2016 Volume: 17 525-534.

[5] Bouain, Mokhtar; Berdjag, Denis; Fakhfakh, Nizar; Atitallah, Rabie Ben. Multi-Sensor Fusion for Obstacle Detection and Recognition: A Belief-Based Approach. 21st International Conference on Information Fusion (FUSION) 2018 1217-1224.

[6] Chadwick, Simon; Maddern, Will; Newman, Paul. Distant Vehicle Detection Using Radar and Vision. IEEE International Conference on Robotics and Automation (ICRA) 2019.

[7] Pinggera, Peter; Ramos, Sebastian; Gehrig, Stefan; Franke, Uwe; Rother, Carsten; Mester, Rudolf. IEEE/RSJ International Conference on Intelligent Robots and Systems (IROS) 2016 1099-1106.

[8] Gupta, Krishnam; Javed, Syed Ashar; Gandhi, Vineet; Krishna, K. Madhava. MergeNet: A Deep Net Architecture for Small Obstacle Discovery. IEEE International Conference on Robotics and Automation (ICRA) 2018 1-7.

[9] Ramos, Sebastian; Gehrig, Stefan; Pinggera, Peter; Franke, Uwe; Rother, Carsten. Detecting unexpected obstacles for self-driving cars: Fusing deep learning and geometric modeling. IEEE Intelligent Vehicles Symposium (IV) 2017 1025-1032.

[10] Xue, Feng; Ming, Anlong; Zhou, Menghan; Zhou, Yu. A Novel Multilayer Framework for Tiny Obstacle Discovery. IEEE International Conference on Robotics and Automation (ICRA) 2019.

[11] Ruff, Todd M. Application of Radar to Detect Pedestrian Workers Near Mining Equipment. Applied Occupational and Environmental Hygiene 2001 Volume: 16 Number: 8 798-808.

[12] Manduchi, R; Castano, A; Talukder, A; Matthies, L. Obstacle detection and terrain classification for autonomous off-road navigation. Autonomous Robots 2005 Volume: 18 Number: 1 81-102.

[13] Furukawa, T.; Bourgault, F.; Lavis, B.; Durrant-Whyte, H.F. Recursive Bayesian SearchandTracking using Coordinated UAVs for Lost Targets. IEEE International Conference on Robotics and Automation (ICRA) 2006 2521-2526.

[14] Hodges, J.; Attia, T.; Doan, L.; Abdelatty, K.; Furukawa, T.; Arukgoda, J.; Ranasinghe, R.; Dissanayake, G.; Kang, C.; Cowden, M. Multistage Bayesian Autonomy for High-Precision Operation in a Large Field. Journal of Field Robotics 2019 Volume: 36 Number: 1 183-203.